

# Merging neutron stars: asymmetric systems

S. Rosswog<sup>1</sup>, M.B. Davies<sup>2</sup>, F.-K. Thielemann<sup>3</sup>, and T. Piran<sup>4</sup>

<sup>1</sup> Center for parallel computing (ZPR/ZAİK), Universität zu Köln, Germany

<sup>2</sup> Department Physics and Astronomy, University of Leicester LE1 7RH, UK

<sup>3</sup> Departement für Physik und Astronomie, Universität Basel, Switzerland

<sup>4</sup> Racah Institute for Physics, Hebrew University, Jerusalem, Israel

Received 2 June 1999 / Accepted 17 May 2000

**Abstract.** We present the results of 3D, Newtonian hydrodynamic calculations of the last stages of the inspiral and the final coalescence of neutron star binary systems. Our focus is on slightly asymmetric systems, where the asymmetry stems from either different masses (1.3 and 1.4  $M_{\odot}$ ) or spins of both components. Almost immediately after contact a fast rotating, very massive central object forms. All calculations exhibit baryonic masses above 2.3  $M_{\odot}$ , thus based on our calculations it is not possible to decide on the fate of the central core of the merged configuration. It might collapse immediately to a black hole, but also the creation of a supermassive neutron star with  $\sim 2.8 M_{\odot}$  cannot firmly be excluded. Depending on the asymmetry of the system the central object receives a kick of several hundred kilometers per second. Different spins of both components do not jeopardize the formation of (to within numerical resolution) baryon free funnels above the poles of the central objects. In the case of different masses the less massive components get disrupted and engulf the more massive companions that stay rather unaffected by the collision. The amount of ejected material is in a similar range as for symmetric systems and could contribute substantially to the enrichment of the Galaxy with heavy r-process elements. Test calculations indicate that the amount of ejected material is basically determined by the high density behaviour of the nuclear equation of state.

Test calculations for the hybrid artificial viscosity scheme that is used for this work are given in the appendix.

**Key words:** hydrodynamics – stars: binaries: close – stars: neutron – gamma rays: bursts

## 1. Introduction

The coalescence of compact binary objects has received such attention since its inspiral is expected to emit gravitational waves in the frequency band that is best accessible to ground based gravitational wave detectors such as LIGO (Abramovici et al., 1992), VIRGO (Bradaschia et al., 1990), TAMA (Kuroda et al., 1997) and GEO600 (Luck, 1997).

In addition this scenario has for many years been “the” model for the central engine to power gamma ray bursts

(GRBs), especially since the final detection of counterparts in wavelength regimes different from gamma rays (Paradijs et al., 1997; Sahu et al., 1997; Galama et al., 1997; Djorgovski et al., 1997; Costa et al., 1997; Frail et al., 1997). However, with the BeppoSAX detection of GRBs with enormous redshifts the situation somehow has changed: even the coalescence of a neutron star binary with its enormous gravitational binding energy of  $\sim 5 \cdot 10^{53}$  erg might not be able to produce  $\sim 3 \cdot 10^{54} \cdot (\frac{\Omega}{4\pi})$  erg in gamma rays ( $\Omega$  is the beaming angle) that are required for the recent burst GRB990123 (Blandford & Helfand, 1999). Now there is growing consensus that the bimodal distribution of burst durations has to be attributed to two different kinds of progenitors. The short ones, that are observationally rather unconstrained due to the BeppoSAX trigger time of five seconds, possibly emerge from accretion disks around black holes resulting from the coalescences of neutron star - neutron star (ns-ns) or low mass black hole - neutron star (bh-ns) systems and the longer ones from the so-called “failed supernovae” (Bodenheimer & Woosley, 1983; Woosley, 1993), “collapsars” or “hypernovae” (Paczynski, 1998; Galama et al., 1998; Iwamoto et al., 1998; Wheeler et al., 1998). Recent simulations (MacFadyen & Woosley, 1999) indicate that in this case indeed a highly energetic jet might be driven through the mantle of the collapsing high-mass star.

Further interest in the merging scenario arises from its possible importance for r-process nucleosynthesis (Lattimer & Schramm 1974, 1976; Symbalisty & Schramm 1982; Eichler et al. 1989; Meyer 1989; Rosswog et al. 1999, hereafter Paper I). Despite a reasonable understanding of the underlying nuclear processes and many years of intense research, it has not yet been possible to identify the corresponding production site unambiguously. The “classical” r-process site, type II supernovae, seem not to be able to provide the entropies required for a reproduction of the solar r-process pattern (Freiburghaus et al., 1997; Freiburghaus et al., 1999a; Meyer & Brown, 1997) unless very special neutrino properties are chosen (McLaughlin et al., 1999). The decompression of low entropy, low  $Y_e$  material could be an alternative or supplementary scenario.

The evolution of the last inspiral stages and the subsequent coalescence of close compact binaries have been dis-

cussed by a number of groups. The first 3D hydrodynamic calculations have been performed by Nakamura and collaborators (see Shibata et al. (1993) and references therein). Similar calculations have been performed by Davies et al. (1994) who discussed a number of physical processes connected with the merging event. Zhuge et al. (1994; 1996) focussed in their work on the emission of gravitational radiation. Lai, Rasio and Shapiro analyzed close binary systems both analytically (Lai et al., 1993a; Lai et al., 1993b; Lai et al., 1994a; Lai et al., 1994b; Lai, 1994; Lai et al., 1994c) as well as with numerical calculations (Rasio & Shapiro, 1992; Rasio & Shapiro, 1994; Rasio & Shapiro, 1995) where their main interest was focussed on stability issues. Many of their results were confirmed by the work of New and Tholine (1997). Ruffert et al. (1996; 1997) were the first to include microphysics (realistic equation of state, neutrino emission) in their hydrodynamic calculations. Rosswog et al. (1999) focussed in their work on the mass loss during the merger event and possible implications for the nucleosynthesis of heavy elements. Recently the interaction of low mass black holes with neutron stars has been investigated (Ruffert & Janka, 1999; Kluzniak & Lee, 1998; Janka & Ruffert, 1998).

Several attempts have been made to include effects of general relativity (GR) in approximative ways, in both analytical (Lai, 1996; Taniguchi & Nakamura, 1996; Lai & Wiseman, 1997; Lombardi et al., 1997; Taniguchi & Shibata, 1997; Shibata & Taniguchi, 1997) and numerical treatments (Wilson & Mathews, 1995; Shibata, 1996; Wilson et al., 1996; Mathews & Wilson, 1997; Baumgarte et al., 1997; Baumgarte et al., 1998a; Baumgarte et al., 1998b; Shibata et al., 1998; Bonazzola et al., 1999). However, the corresponding results are still not free of controversies. Recently attempts have been made to give an SPH-formulation of the Post-Newtonian formalism of Blanchet, Damour and Schäfer (1990) (Ayal et al., 1999; Faber & Rasio, 1999).

After having concentrated in previous simulations on symmetric neutron star binary systems we want to focus in this investigation on slightly asymmetric neutron star binaries. Neutron star systems with mass ratio  $q \neq 1$  have previously been analyzed by Rasio and Shapiro (1994) and Zhuge et al. (1996). However, both groups used simple polytropes to approximate the equation of state, whereas in the work reported here we use the realistic nuclear equation of state of Lattimer & Swesty (1991).

The ingredients of our model are described in Sect. 2, results concerning morphology, mass distribution, kick velocities of the central objects, possible implications for GRBs, temperatures and ejecta may be found in Sect. 3. A summary and discussion of our results are given in Sect. 4.

## 2. The model

### 2.1. The numerical method

We solve the dynamic equations of fluid motion in three dimensions using the smoothed particle hydrodynamics (SPH)

method. Due to its Lagrangian nature this method is perfectly suited to tackling this intrinsically three dimensional problem. It is not restricted to a computational domain imposed by a grid and it is easy to track the history of chosen blobs of matter (e.g. ejected material). Since this method has been discussed extensively, we restrict ourselves here to mentioning just the basic ingredients of our code and refer to the literature for further details (see e.g. Hernquist and Katz (1989), Benz (1990) and Monaghan (1992)).

The Newtonian gravitational forces are evaluated using a hierarchical binary tree as described in Benz et al. (1990). The additional forces arising from the emission of gravitational waves will be discussed below.

### 2.2. Gravitational radiation backreaction

Since the forces emerging from the emission of gravitational waves tend to circularize binary orbits, we start our calculations with circular orbits (Peters & Mathews, 1963; Peters & Mathews, 1964) and add the radial velocity of a point-mass binary in quadrupole approximation (see e.g. Shapiro & Teukolsky (1983)):

$$\frac{da}{dt} = -\eta a, \quad \eta = \frac{64}{5} \frac{G^3}{c^5} \frac{M^2 \mu}{a^4}, \quad (1)$$

where  $a$  is the distance between the binary components,  $M$  the total and  $\mu$  the reduced mass of the system. In addition to the accelerations from hydrodynamic and Newtonian gravitational forces we apply to each SPH-particle in star  $i$  the backreaction acceleration  $\mathbf{a}_{gwb,i}$  found for a point-mass binary with unequal masses  $M_1$  and  $M_2$ . Starting from the point mass formulae for the loss of energy  $E$  and angular momentum  $\mathbf{J}$  due to the emission of gravitational waves on circular orbits,  $\frac{dE}{dt} = \eta E$  and  $\frac{d\mathbf{J}}{dt} = -\frac{\eta}{2} \mathbf{J}$ , and assuming  $\frac{dE}{dt} = \sum_i m_i \mathbf{v}_i \cdot \mathbf{a}_{gwb,i}$  and  $\frac{d\mathbf{J}}{dt} = \sum_i m_i \mathbf{x}_i \times \mathbf{a}_{gwb,i}$ , we derive

$$\ddot{x}_{i,gwb} = (-1)^{i+1} \frac{\eta}{M_i (\mathbf{r}_{12} \cdot \mathbf{v}_{12})} \left( E x_{12} + \frac{J \dot{y}_{12}}{2} \right) \quad (2)$$

$$\ddot{y}_{i,gwb} = (-1)^{i+1} \frac{\eta}{M_i (\mathbf{r}_{12} \cdot \mathbf{v}_{12})} \left( E y_{12} - \frac{J \dot{x}_{12}}{2} \right). \quad (3)$$

Here  $\mathbf{r}_{12} = \mathbf{r}_1 - \mathbf{r}_2$ ,  $\mathbf{v}_{12} = \mathbf{v}_1 - \mathbf{v}_2$  and their components are  $x_{12}, y_{12}; \dot{x}_{12}, \dot{y}_{12}$ . For systems with equal masses this reduces to the formula given in (Davies et al., 1994). The backreaction acceleration is switched off when the stars come into contact and the point mass limit is definitely inappropriate. In test calculations our backreaction force has been compared to the frictional force of (Zhuge et al., 1996), where the accelerations were calculated according to

$$\mathbf{a}_{gwb,1} = -\frac{G}{2} \frac{M_1 \mu}{M_2 a} \eta \frac{\mathbf{v}_1}{|\mathbf{v}_1|} \quad (4)$$

for star 1 and similar for star 2. The results found for both implementations were almost indistinguishable. A further discussion concerning the appropriateness of this approach may be found in Paper I.

**Table 1.** Summary of the different runs: *spin*: 1: no spin + spin with orbit; 2: no spin + spin against orbit; 3: no spin + spin in orbital plane 1; 4: corotation; 5: no stellar spins; 6: spins against orbit (Fig. 1). Masses are given in solar units. LS: Lattimer & Swesty (1991).  $\Gamma_1$  and  $\Gamma_2$  refer to the adiabatic index of the pseudo-polytropic EOS given in Eq. (8). AV refers to the artificial viscosity scheme,  $E_{s.o.}$  to the total energy at the time when the backreaction force is switched off,  $E_{fin}$  at the end of the calculation.

run	spin	$M_1$	$M_2$	# part.	$a_0$ [km]	EOS	initial equilibrium	AV	$ E_{s.o.} - E_{fin} / E_{fin} $
A	1	1.4	1.4	20000	45	LS	no	hybrid	$3.1 \cdot 10^{-4}$
B	2	1.4	1.4	20000	45	LS	no	hybrid	$6.0 \cdot 10^{-4}$
C	3	1.4	1.4	20000	45	LS	no	hybrid	$1.3 \cdot 10^{-3}$
D	4	1.3	1.4	20000	45	LS	yes	hybrid	$9.8 \cdot 10^{-4}$
E	5	1.3	1.4	20000	45	LS	no	hybrid	$1.1 \cdot 10^{-4}$
F	6	1.3	1.4	20852	45	LS	no	hybrid	$9.0 \cdot 10^{-4}$
G	4	1.6	1.6	20974	45	$\Gamma_1 = 2.0, \Gamma_2 = 2.6$	no	standard	$5.9 \cdot 10^{-4}$
H	4	1.6	1.6	20000	45	$\Gamma_1 = 2.6, \Gamma_2 = 2.0$	no	standard	$2.6 \cdot 10^{-3}$
I	5	1.3	1.4	20000	45	LS	no	standard	$3.1 \cdot 10^{-4}$
J	5	1.3	1.4	20000	45	LS	no	no	$1.3 \cdot 10^{-3}$

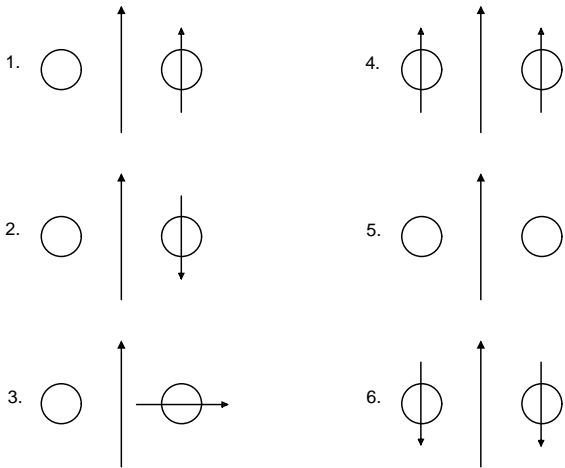


**Fig. 1.** The investigated spin orientations. The large arrow symbolizes the orbital and the small one the spin angular momentum.

### 2.3. Artificial viscosity

The probably-superfluid, almost inviscid neutron star material poses a severe problem for a numerical simulation. In addition to the numerical dissipation arising from discretisation, SPH uses an artificial viscosity (AV) to resolve shocks properly. The standard form of AV (Monaghan, 1992) is known to yield good results in pure shocks but to introduce spurious entropy generation in shear flows (for an extensive report on the effects of AV see (Lombardi et al., 1999)). In this work a new, hybrid scheme of AV is used that profits from two recently suggested improvements: the decrease of the viscosity parameters to low minimum values in the absence of shocks (Morris & Monaghan, 1997) and the so-called Balsara-switch (Balsara, 1995) to reduce viscosity in pure shear flows. Details and test calculations of the new hybrid scheme are given in the appendix.

### 2.4. The nuclear equation of state

The equation of state (EOS) of the neutron star material is an important ingredient of the model, but unfortunately it is only

poorly known and thus introduces large uncertainties into the calculation. In Paper I we found, for example, that the amount of ejected mass is very sensitive to the stiffness, i.e. the adiabatic exponent, of the EOS.

To describe the macroscopic properties of the neutron stars we use for our calculations the temperature dependent equation of state of Lattimer and Swesty (1991) in a tabular form. This EOS models the hadronic matter as a mixture of a heavy nucleus (representative for an ensemble of heavy nuclei), alpha particles (representing light nuclei) and nucleons outside nuclei. To mimic the softening of the EOS at high densities resulting from the appearance of “exotic” particles (such as hyperons, kaons and pions), which are neglected in the approach of Lattimer and Swesty, we use the lowest available compressibility,  $K = 180$  MeV. Technical details concerning the EOS may be found in Appendix B of Paper I.

### 2.5. Masses

All known neutron star binary systems show a remarkably small mass difference between the two components (e.g. Thorsett (1996); Thorsett and Chakrabarti (1999)). The maximum known mass difference is  $\approx 4\%$  for PSR 1913+16. However, the overall dynamics of the merging event is rather sensitive to those mass differences (see e.g. Rasio and Shapiro (1994)) and larger asymmetries in the masses cannot be excluded on grounds of the five known systems.

In the cases where we are interested in the question of how unequal neutron star spins alter previous results, we study binary systems where both components have a baryonic mass of  $1.4 M_{\odot}$  (for details see Table 1). To examine the effects of unequal masses we consider systems containing a  $1.3 M_{\odot}$  and a  $1.4 M_{\odot}$  star. Keeping in mind that the well-known systems are centered around  $1.35 M_{\odot}$  this choice is highly realistic.

### 2.6. Stellar spins

Bildsten and Cutler (1992) and Kochanek (1992) have shown that the internal viscosity of the neutron star material is by far too

low for a tidal locking of both components within the short time scale during which the stars can tidally interact. They concluded that the system should be close to irrotational, i.e. spin angular momentum should be negligible in comparison to the orbital angular momentum. Observationally there is not very much known about spin distributions in neutron star binary systems. We regard it an interesting question whether the amount of ejected mass is altered decisively by unequal stellar spins. The tremendous interest in the coalescence scenario of two neutron stars has been triggered -among other reasons- by its possible connection to the still poorly understood GRBs. After a decade as *the* model for the central engine of GRBs it is currently favoured as the most promising model for (at least) the subclass of short bursts. One of the features that makes this scenario appealing is the emergence of baryon free funnels above the polar caps of the central object, which have been found in the calculations of symmetric systems (Davies et al., 1994; Ruffert et al., 1997; Rosswog et al., 1999). These funnels are attractive sites for the fireball scenario since they are close to the central source but relatively free of baryons, which could prevent the emergence of GRB (Shemi & Piran, 1990).

Here we investigate cases where both components carry different spins to see if these baryon free funnels still emerge. We analyze systems where one member carries no spin and the other star either rotates with the angular frequency of the orbit in the same direction as the orbit (spin parallel to the orbital angular momentum), opposite to it (antiparallel to the orbit) or with the spin lying in the orbital plane (see Fig. 1). In each case the spin frequencies are set equal to the orbital frequency at the initial separation ( $a_0 = 45$  km), corresponding to a spin period of 2.9 ms.

### 2.7. Tidal deformation

When a ns binary system has spiralled down to a distance corresponding to our initial separation (45 km) the deformation due to mutual tidal forces will be of the order  $\delta R \approx R^4 a_0^{-3} \approx 0.5$  km and thus non-negligible. For corotating systems the construction of accurate numerical initial models is rather straight forward since in a frame corotating with the binary the fluid velocities vanish. Thus, following Rasio and Shapiro (1992), we force the system to relax into a corotating equilibrium state by applying an artificial friction force proportional to the particle velocities. Details of our approach are described in Paper I.

For the non-corotating binaries we started our calculations with spherical stars. These are only very approximate initial conditions and thus starting with spherical stars leads to oscillations during the inspiral phase with a frequency given by  $\omega_{\text{osc}} \approx 2\pi(G\bar{\rho})^{1/2}$ . In Paper I the effects resulting from the oscillations have been investigated carefully. They were found to increase the temperatures and internal energies of the final configuration, but had a negligible influence on the mass distribution. Thus we regard spherical stars at the beginning of our calculations as a good approximation for the purposes of this work.

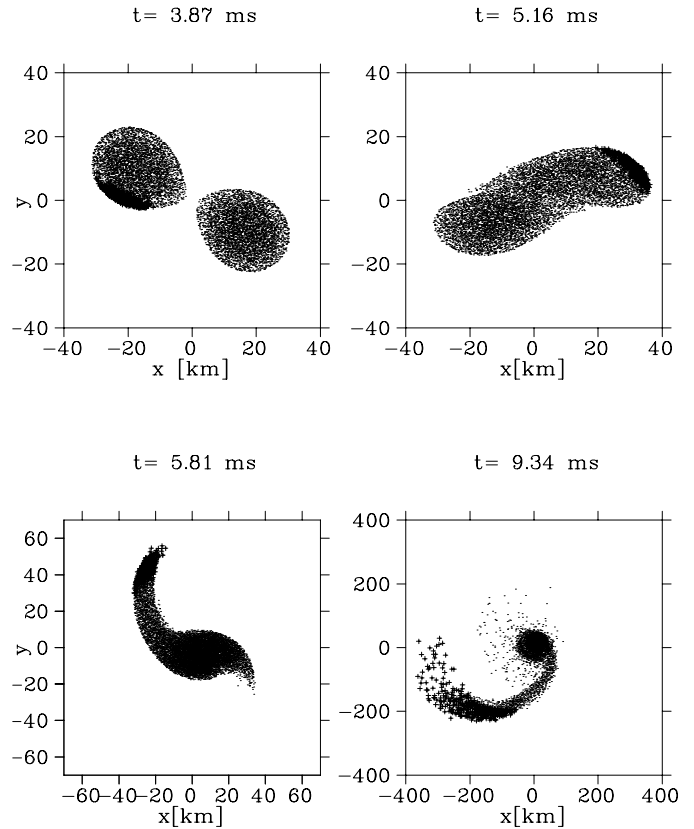


**Fig. 2.** Morphology of a corotating binary system with neutron stars of masses  $1.3$  and  $1.4 M_{\odot}$  (run F). Dots indicate projections of particle positions onto the orbital plane, crosses show particles that are unbound at the end of the simulation.

## 3. Results

Our calculations start with initial separations  $a_0 = 45$  km and follow the last stages of the inspiral and the final coalescence over 12.9 ms. The characteristics of the investigated cases are summarized in Table 1. The total energy (after switching off the gravitational wave backreaction force) is typically conserved to a few times  $10^{-4}$  (see column 8 in Table 1).

### 3.1. Morphology

Our runs can be separated into two groups: for the first group (run A - run C) the asymmetry of the system is introduced by individual spins of the stars, for the second group (run D - run F) it is given by different masses of the components.

In run A (where one ns had no spin and the other was spinning parallel to the orbital angular momentum) two spiral arms of different size are formed after the coalescence. These get wrapped around the central object, hit its surface supersonically and result in a thick, toroidal, shock-heated disk. The final configuration consists of a massive central object, and a thick disk surrounded by asymmetrically-distributed rapidly-expanding low density material.

In case B, where the star with spin rotates against the orbital motion, the emerging spiral arms are less well-defined and

**Table 2.** Masses of the different morphological regions (‘co’ stands for central object, ‘ld’ for the low density parts outside the disk),  $\tilde{M}_{\text{co}}$  is a lower limit on the gravitational mass (see Eq. (5)) and  $a$  is the relativistic stability parameter (see text).

run	$M_{\text{co}}$ [ $M_{\odot}$ ]	$\tilde{M}_{\text{co}}$ [ $M_{\odot}$ ]	$a$	$M_{\text{disk}}$ [ $M_{\odot}$ ]	$M_{\text{ld}}$ [ $M_{\odot}$ ]
A	2.55	2.13	0.61	0.20	0.05
B	2.69	2.22	0.64	0.10	0.01
C	2.60	2.17	0.60	0.14	0.06
D	2.37	2.00	0.55	0.23	0.10
E	2.49	2.08	0.59	0.16	0.05
F	2.65	2.19	0.66	0.05	$3 \cdot 10^{-3}$

quickly transform into a thick torus of neutron rich material around the central object. In the final configuration the spiral structure has completely dissolved.

In Run C, where the spin of the ns is lying in the orbital plane, spiral arms show up for a very short time ( $\sim 4$  ms) and then transform into a torus engulfing the central object. At the end of the simulation the central object is surrounded by a thick, dense neutron torus ( $\rho \sim 10^{12} - \sim 3 \cdot 10^9 \text{ g cm}^{-3}$ ) that extends to  $\sim 100$  km which itself is embedded into a extended cloud of low-density neutron star debris. In this case the material distribution is tilted by a small angle  $\varphi$  away from the original orbital plane (see Fig. 3). This can be explained easily in terms of angular momentum. If we approximate the rotating star by a rigid, homogeneous sphere rotating with the orbital frequency  $\omega$ , then we find for our initial conditions  $L_{\text{spin}} / L_{\text{orbit}} = 4/5(R/a)^2 \approx 4/5(15\text{km}/45\text{km})^2 = 4/45$ . This translates into an angle of  $\varphi = \arctan(\frac{L_{\text{spin}}}{L_{\text{orbit}}}) \approx 5^\circ$ , which is consistent with the numerical result.

In the second group (where the masses of the ns are 1.3 and 1.4  $M_{\odot}$ ) both stars carry the same spin: in the direction of the orbital motion (since we always use  $\omega_{\text{spin}} = \omega_{\text{orbit}}(a_0)$  this corresponds to corotation; Run D), both stars without spin (irrotational configuration; Run E) or both are spinning against the orbital motion (Run F). In the case of the corotating and irrotational configurations only one spiral arm forms from the material of the less-massive component. In the last case (spins against the orbit) no such spiral structure ever emerges during the whole evolution. Immediately, a very massive central object, engulfed by low density neutron star debris is formed.

### 3.2. Mass distribution

The baryonic masses of the central objects, the tori and the low density regions can be found in Table 2. We use the relation between binding energy and gravitational mass of (Lattimer & Yahil, 1989) for an estimate of a lower limit on the gravitational mass  $\tilde{M}_{\text{co}}$  of our central objects:

$$\frac{\tilde{M}_{\text{co}}}{M_{\odot}} = 5.420 \cdot \left( -1 + \sqrt{1 + 0.369 \frac{M_{\text{b}}}{M_{\odot}}} \right), \quad (5)$$

where  $M_{\text{b}}$  is the baryonic mass. The corresponding values for the central objects are given in the third column of Table 2.

Despite the fact that the observed neutron star masses are all consistent with a narrow Gaussian distribution with  $m_{\text{ns}} = 1.35 \pm 0.04 M_{\odot}$  (Thorsett & Chakrabarti, 1999), present state of the art nuclear EOS allow for much higher neutron star masses, which could possibly indicate that the masses in radio pulsar binary systems might be given rather by evolutionary constraints than by nuclear physics. For example, Weber and Glendenning (1992) found maximum masses for rotating neutron stars of  $\sim 2.5 M_{\odot}$ , most recent investigations (Shen et al., 1998; Akmal et al., 1998) find upper limits for non-rotating stars of  $\sim 2.2 M_{\odot}$  which correspond to the results of Weber and Glendenning if a 20% rotational effect (see e.g. Shapiro and Teukolsky (1983) is added. The gravitational masses  $\tilde{M}_{\text{co}}$  (see Table 2) for the central objects are in the critical range between 2.0 and 2.2  $M_{\odot}$  (note that the baryonic masses of the initial stars are lower (1.3 and 1.4  $M_{\odot}$ ) than in Paper I (1.4 and 1.6  $M_{\odot}$ )). The relativistic stability parameter  $a = (Jc)/(GM^2)$  ((Stark & Piran, 1985); see column 4 in Table 2) is around 0.6 and thus substantially lower than the critical value  $a_{\text{crit}} \approx 1$ , i.e. the increase of the maximum mass resulting from rotational support is negligible. Thus several scenarios are possible. Depending on the maximum neutron star mass the central object could collapse immediately after the merger to a black hole. If the thermal pressure of the hot central object prevents an instantaneous collapse to a black hole it could be stabilized on a neutrino cooling time scale (a few seconds) and then collapse when the thermal pressure support is reduced sufficiently. A third possibility is that the central object is stable even after the neutrinos have diffused out. The collapse could then be triggered by material accreted from the disk on a time scale determined by the largely unknown disk viscosity. It has to be stressed, however, that a secure upper limit on the neutron star mass from causality arguments (Kalogera & Baym, 1996) is as high as 2.9  $M_{\odot}$ . Since our total baryonic mass is  $\leq 2.8 M_{\odot}$  there is still the possibility that a ns remains stable having accreted the thick disk (up to a few tenth of a solar mass) and at least those parts of the surrounding low-density material that are not ejected (see below). This scenario would result in supermassive (around twice the ‘‘canonical’’ value of 1.4  $M_{\odot}$ ), fast rotating, hot neutron stars as an outcome of the coalescence.

### 3.3. Kick velocities

As described in Paper I, symmetric systems retain their symmetry with respect to the origin during the whole merger evolution. The position of the final central object thus coincides with the center of mass of the whole mass distribution. Here, however, due to asymmetries introduced either by different spins or masses of both components, the final mass configuration is not symmetric with respect to the origin anymore and the central object receives a kick through the ejection of high velocity, low density material.

- We find large values of  $v_{\text{kick}}$  for the corotating system with different masses (run D;  $\sim 600 \text{ km s}^{-1}$ ), the case where one ns is spinning in the orbital plane (run C;  $\sim 200 \text{ km s}^{-1}$ ) and the system where only one component is fast rotating with

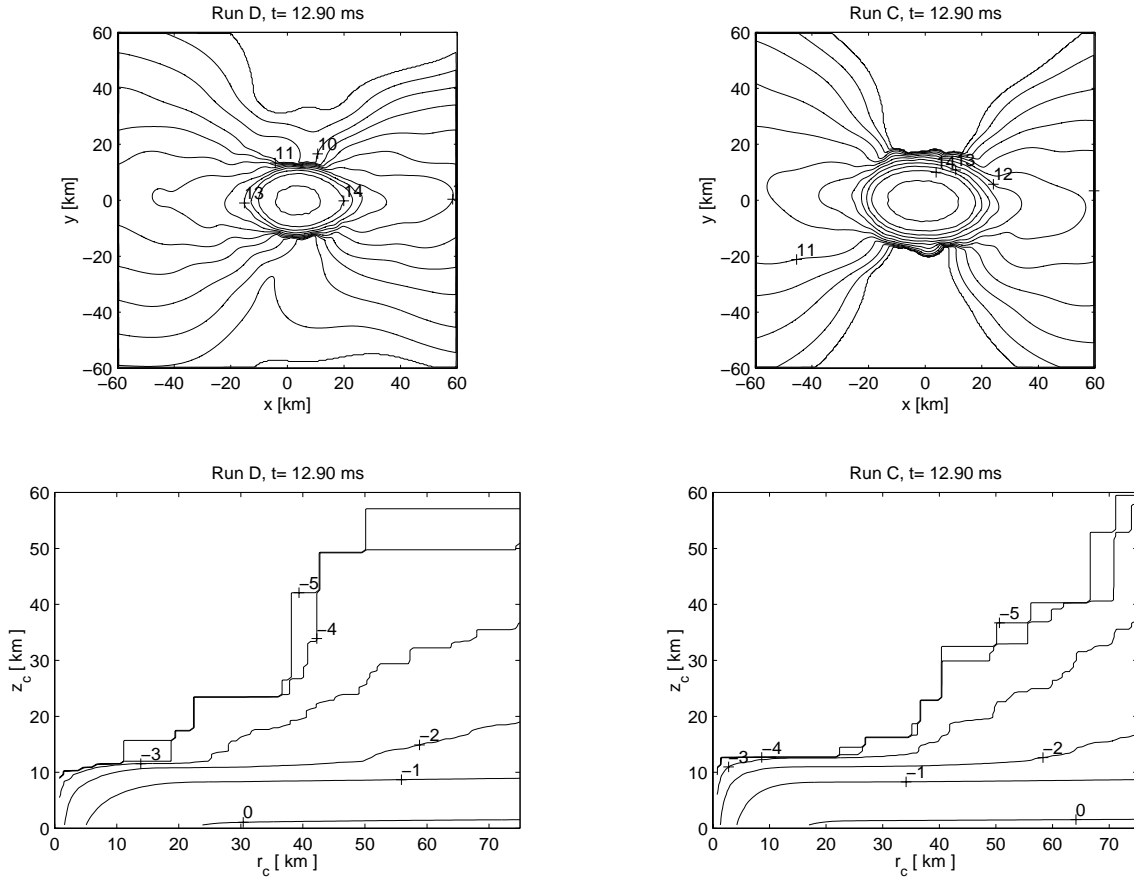


**Fig. 3.** Cut through  $xz$ -plane (at the end of the calculation) of the corotating system (run D; left column) and the one where one spins lies in the orbital plane (run C; right column). The labels in the first line of plots indicate the logarithm of the density contours (in  $\text{g cm}^{-3}$ ). In the lower plots a point at  $(r_c, z_c)$  on a contour line of value  $c$  indicates that a cylinder of radius  $r_c$  along the  $z$ -axis from  $z_c$  to infinity contains less than  $c$  of baryonic material.

the orbital motion (run A;  $\sim 200 \text{ km s}^{-1}$ ). The other initial configurations lead to substantially smaller kicks ( $\sim 100 \text{ km s}^{-1}$ ). Thus the merger of asymmetric neutron star binaries may result in black holes or supermassive neutron stars with kick velocities of several hundred kilometers per second.

### 3.4. Baryonic pollution/GRBs

It was suggested that the funnels that form above the poles of the central objects in symmetric systems would be a natural site for a GRB fireball to form, since these regions were found to be practically free of baryons. It has been thought for a long time that the emergence of a GRB from a region “contaminated” with baryons is impossible. If spherical symmetry is assumed, an amount as small as  $10^{-5} M_{\odot}$  of baryonic material injected into the fireball is enough to prevent a GRB from forming. It was only recently that detailed 3D-calculations in the context of the collapsar-model (MacFadyen & Woosley, 1999; Aloy et al., 1999) have shown that under certain conditions still large relativistic gamma factors can be achieved despite a considerable baryonic loading.

At present it is still an open question whether the mechanism found for the collapsar-model also works in the case neu-

tron star coalescence. It is therefore an interesting question to ask whether the region above the poles of the coalesced object remains free of baryons if the initial neutron star spins are not aligned with the orbital angular momentum. To our knowledge only calculations exist where the stellar spins are aligned, i.e. parallel or antiparallel, with the orbital angular momentum. It is one of the motivations of this investigation to see whether this changes in the case of asymmetric systems. Clearly, the stellar spins only contribute moderately to the total angular momentum of the system ( $\sim 10\%$ , see above) and so changing the stellar spins cannot be expected to overturn the overall picture of the merger, but in case the collapsar mechanism should not work even a small amount of baryonic material might be decisive for the fate of the fireball.

In Fig. 3 we show density contours (from  $\log(\rho_{[\text{g cm}^{-3}]}) = 14.5$  down to 9) in the  $xz$ -plane (i.e. orthogonal to the original orbital plane). We find that changing the stellar spins does not endanger the formation of the baryon free funnel above the polar caps of the central object. However, there are indications that in the case of corotation with different masses more material is found close to the rotation axis. In the calculation of the density contours the smoothing lengths enter and these are in SPH generally evolved in a way such that the number of neighbours

## Max. temperatures

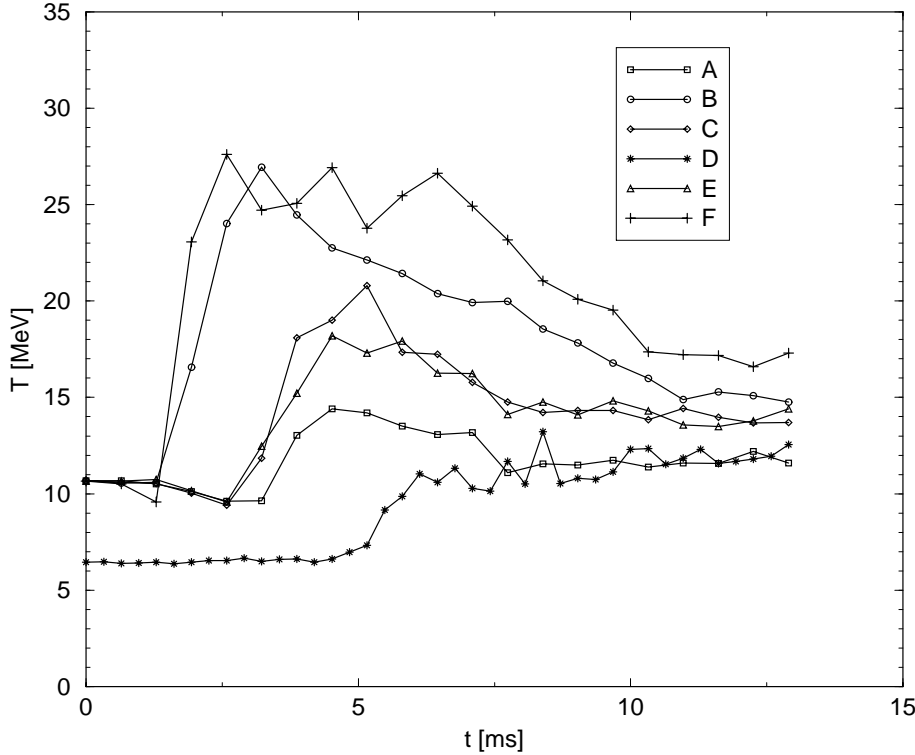


**Fig. 4.** Maximum temperatures of the different runs.

of each particle is kept approximately constant, thus the low density contours are somewhat biased by the resolution.

For the two lower panels of Fig. 3 only the particle masses and their corresponding positions were used. They are intended to give an idea of the particle masses that are contained in a cylinder positioned above the pole starting with height  $z_c$  and radius  $r_c$ . Thus a point at  $(r_c, z_c)$  on a contour line of value  $c$  indicates that a cylinder of radius  $r_c$  along the  $z$ -axis from  $z_c$  to infinity contains *less* than  $c$  of baryonic material. These plots reflect that more mass is found close to the rotation axis in the case of a corotating system with  $q \neq 1$ . However, on the one hand these indications are biased by the current numerical resolution and on the other hand the corotating case is unlikely to be encountered in reality. Since in the most realistic case (where the ns have masses  $1.3$  and  $1.4 M_\odot$  and no spins; run E) the polar regions are still free of baryons this place still has to be regarded as an excellent site for the emergence of a fireball.

### 3.5. Temperatures

Low temperatures in the degenerate regime are numerically difficult to determine since even the slightest noise in the internal energy density, which is our independent variable, can lead to appreciable staggering in the temperature. However, this does not influence the dynamical evolution in any way.

Similar to the symmetric cases (see Ruffert et al. (1996), Paper I) vortex rolls form along the contact interface as soon as the stars merge (for a more detailed discussion see Paper I).

The vortex sheet emerging at the contact interface is Kelvin-Helmholtz unstable on all wavelengths and therefore difficult to model in a 3D calculation (see e.g. Rasio and Shapiro (1999)). The maximum temperatures of the systems are found in these vortices. These are highest for the cases with the most shear interaction (spin against orbital motion, run F and B) where peak temperatures above  $\sim 25$  MeV are found (note that due to the lower total mass the mergers are less violent than the ones described in Paper I). The lowest temperatures are found in the corotating case (run D). One reason is that -due to the initial relaxation- the system practically does not oscillate during the inspiral. The other reason is that this case exhibits the minimum shear motion (zero velocity in the corotating frame) of all cases. The evolution of the peak temperatures of the different cases are shown in Fig. 4.

The thick disks are created when the spiral arms are wrapped up around the central object. During this process different parts of the spiral arms collide supersonically and their inner parts hit the surface of the central object. The shock heated disks have in all cases mean temperatures between 3 and 4 MeV. Due to the shear motion within the disk artificially high temperatures as artifacts of the artificial viscosity cannot be fully excluded, not even with our new viscosity scheme (see appendix) which exhibits a strongly improved behaviour in shear flows. Thus, these temperatures should be regarded as an upper limit to the true disk temperatures. Our results for the temperatures are close to those reported by Ruffert et al. (1996) for their PPM-calculations.

### 3.6. Ejecta

In part the enormous interest in the coalescence scenario of two neutron stars arises from its possible importance for nucleosynthesis. Despite intense research it has not been possible to pin down the astrophysical production site of the r-process nuclei. For their production these nuclei basically need an environment which is characterized by the presence of seed nuclei and very high neutron densities. These conditions are suggestive of explosive events in neutron-rich surroundings. The most popular scenario is a type II supernova. However, recent calculations reveal two severe problems connected with this production site: (i) there is no way to produce the observed r-process abundance pattern for nucleon numbers below 120 (Freiburghaus et al., 1997; Freiburghaus et al., 1999a) and (ii) the nuclei above this value can only be reproduced if entropies are applied that exceed the entropy values of “state-of-the-art” supernova calculations by a factor of 3 to 5 (Takahashi et al., 1994; Meyer & Brown, 1997; Hoffman et al., 1997; Meyer et al., 1998; Freiburghaus et al., 1999a). The only possible way out from this conclusion would be the introduction of sterile neutrinos (see e.g. McLaughlin (1999)).

The neutron star merger scenario is a promising r-process site since it provides in a natural way the neutron rich environment needed for the capture reactions.

To clarify the importance of the merger scenario for the r-process nucleosynthesis the following questions have to be answered: (i) how often do such mergers occur? (ii) how much mass is (depending of the parameters of the binary system) ejected per event? and (iii) how much of this material is r-process matter, respectively, do we find a solar r-process pattern? Here we focus on the second point. The third one has been discussed in a recent paper (Freiburghaus et al., 1999b).

Since at the end of our calculations the outermost parts of the neutron star debris are basically ballistic, it is a reasonable approximation to treat the SPH-particles as point masses in the gravitational potential of the central mass distribution. Replacing the central mass by a point mass  $M$ , we can calculate the orbital eccentricities of the point masses  $m_i$ :

$$e_i = \sqrt{1 + \frac{2E_i J_i^2}{G^2 m_i^3 M^2}}, \quad (6)$$

where  $E_i$  and  $J_i$  are energy and angular momentum of particle  $i$ . A particle  $i$  is regarded as being unbound if  $e_i > 1$ . Since the assumption of ballistic motion may possibly not be justified everywhere we test the results by calculating the sum of each particle’s energies (see Paper I). The amounts of ejected material according to both criteria are in good agreement and are given in Table 3.

We find that the ejecta for asymmetric coalescences are comparable to those from symmetric systems (see Paper I). The only larger deviation is found for the case where both neutron stars spin against the orbital motion. Here we can hardly resolve any mass loss ( $\sim 2 \cdot 10^{-4} M_\odot$ ) while the corresponding spin configuration in Paper I ejected  $\sim 5 \cdot 10^{-3} M_\odot$ . This larger value

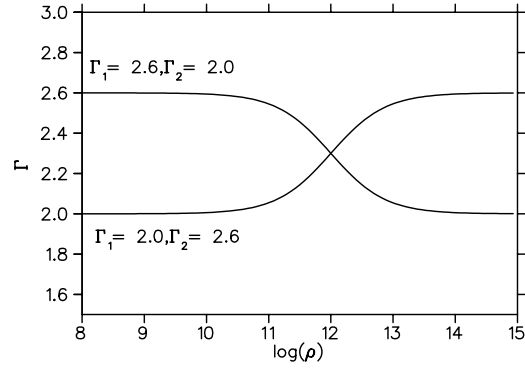


**Fig. 5.** Dependence of the adiabatic index on density for the pseudo-polytropic EOS used in the test runs H and J.

may be a result of spurious entropy generation by the former artificial viscosity that is now suppressed by our new scheme (see appendix). However, this configuration is very unlikely to be encountered in nature and only meant to give a lower limit for the spin dependence of the ejecta. To be cautious we have explored the dependence of these results on the AV with two further test runs: we start from the initial conditions of the most probable initial configuration, run E, but use the standard AV scheme in one case and in the other we use no AV. With the standard AV we find that  $\sim 20\%$  more material is ejected; without AV the result is practically the same as was obtained with our hybrid scheme. Thus, the mass loss measured in this paper is *definitely not an artifact of the AV scheme*. The ejecta for the other configurations range from a few times  $10^{-3} M_\odot$  to a few times  $10^{-2} M_\odot$  exhibiting a strong sensitivity to the stellar spins.

It has to be stressed again that the amount of ejected material is crucially dependent on the poorly known nuclear equation of state. In test runs using a soft polytrope ( $\Gamma = 2.0$ ) we were not able to resolve any mass loss at all (Paper I). To test the sensitivity of the amount of ejecta on the behaviour of the EOS in different density regimes we performed two additional test runs. In both of these runs we used a polytropic EOS whose adiabatic exponent  $\Gamma$  varies with density  $\rho$ :

$$P = (\Gamma(\rho) - 1)\rho u, \quad (7)$$

where  $P$  denotes the pressure and  $u$  the specific internal energy. The adiabatic exponent was prescribed according to

$$\Gamma = \Gamma_1 - (\Gamma_1 - \Gamma_2) \left( \frac{\rho}{\rho + \rho_0} \right). \quad (8)$$

We chose  $\rho_0 = 10^{12} \text{ g cm}^{-3}$  and took the values from Paper I (2.0 and 2.6) for  $\Gamma_1$  and  $\Gamma_2$  (see Fig. 5). In the first case (run G), the high density part of matter followed a  $\Gamma = 2.6$ -polytrope whereas the low density material was governed by a  $\Gamma = 2.0$ -polytrope. In the second case (run H) the polytropic indices were switched. This allowed us to start from the initial configuration of runs C and K of Paper I and thus assured that changes in the amount of ejecta are exclusively due to variations in  $\Gamma$ . Both cases indicate that the results (see Table 3) are governed by the central part of the merged configurations, i.e. *the behaviour of*

**Table 3.** Amount of ejected material (masses are given in solar units).

run	remark	$m_{\text{ej}}$ (# part.), $e_i > 1$	$m_{\text{ej}}$ (# part.), $E_{i,\text{tot}} > 0$
A	1.4 & 1.4 $M_{\odot}$ , spin: 1	$1.49 \cdot 10^{-2}$ (134)	$1.42 \cdot 10^{-2}$ (128)
B	1.4 & 1.4 $M_{\odot}$ , spin: 2	$2.66 \cdot 10^{-3}$ (24)	$2.66 \cdot 10^{-3}$ (24)
C	1.4 & 1.4 $M_{\odot}$ , spin: 3	$1.70 \cdot 10^{-2}$ (164)	$1.74 \cdot 10^{-2}$ (168)
D	1.3 & 1.4 $M_{\odot}$ , spin: 4	$3.64 \cdot 10^{-2}$ (390)	$3.62 \cdot 10^{-2}$ (387)
E	1.3 & 1.4 $M_{\odot}$ , spin: 5	$1.11 \cdot 10^{-2}$ (99)	$1.14 \cdot 10^{-2}$ (101)
F	1.3 & 1.4 $M_{\odot}$ , spin: 6	$2.0 \cdot 10^{-4}$ (2)	$3.1 \cdot 10^{-4}$ (3)
G	1.6 & 1.6 $M_{\odot}$ , spin: 4	$1.93 \cdot 10^{-2}$ (160)	$2.07 \cdot 10^{-2}$ (172)
H	1.6 & 1.6 $M_{\odot}$ , spin: 4	0 (0)	$1.21 \cdot 10^{-4}$ (2)
I	like run E, std. AV	$1.36 \cdot 10^{-2}$ (134)	$1.35 \cdot 10^{-2}$ (132)
J	like run E, no AV	$1.13 \cdot 10^{-2}$ (98)	$1.15 \cdot 10^{-2}$ (100)

the nuclear equation of state in the high density regime basically determines the amount of ejected neutron star debris. This is unfortunately the poorest known regime of the EOS and reveals again that tighter limits on the stiffness of the EOS would be highly desirable. In addition, this sensitivity to the strong field gravitational potential in the center of the mass distribution indicates that we are at the limit of applicability of Newtonian gravity and thus further calculations including general relativistic gravity are necessary.

#### 4. Summary and discussion

We have presented Newtonian, 3D calculations of the hydrodynamic evolution of neutron star binary coalescences where we have used the smoothed particle hydrodynamics method coupled to the realistic nuclear equation of state of Lattimer and Swesty. Our focus in this investigation was on slightly asymmetric binary systems, where the asymmetry stemmed either from different masses (1.3 and 1.4  $M_{\odot}$ ) or spins of both components (both stars of mass 1.4  $M_{\odot}$ ).

In all cases a fast rotating central object with a baryonic mass above  $2.3M_{\odot}$  formed. Since the exact maximum neutron star mass is unknown and our calculations are Newtonian we cannot decide on the fate of the central object. It might collapse to a black hole directly after the merger, but it might instead remain stable on a neutrino diffusion or an accretion time scale (determined by the largely unknown disk viscosity). Even the final creation of supermassive neutron stars with twice the canonical mass value of 1.4  $M_{\odot}$  cannot firmly be excluded.

The central object is surrounded by a thick disk containing between 0.05 and 0.23  $M_{\odot}$ . Typically a few percent of a solar mass is in rapidly expanding low density regions. In the cases where this low density material is expelled in an asymmetric way, the central object receives a kick velocity of several hundred kilometers per second (we found the highest kick velocities of  $\sim 600 \text{ km s}^{-1}$  for a corotating system containing a 1.3 and a 1.4  $M_{\odot}$  star), which is comparable to the kick velocities of neutron stars that result from asymmetric supernova explosions (e.g. Fryer and Kalogera (1997)), Fryer et al. (1998)).

One motivation to study systems with neutron star spins that are *not* orthogonal to the orbital plane was to see whether the baryon free funnels above the poles of the central objects that

have been found in previous calculations are “polluted” by the injection of baryonic material. However, we did not observe such an effect. Funnels similar to the symmetric cases arose for all spin combinations. For the cases with the neutron star spins lying in the orbital plane the final disk was tilted by a small angle with respect to the original orbital plane.

As found in earlier investigations (Rasio & Shapiro 1994) even small deviations from the mass ratio  $q = 1$  result in dramatic consequences for the overall hydrodynamic evolution of the systems. Here we have investigated systems of 1.3 and 1.4  $M_{\odot}$  ( $q \approx 0.93$ ). The heavier star was rather unaffected by the coalescence whereas the lighter one was disrupted, forming a layer of debris around the heavier and providing the material for the formation of the low density regions (spiral arms, disks). For initial corotation parts of this debris are driven towards the rotation axis. However, since corotating ns binaries are very unlikely and in the more probable spin configurations baryon free funnels appear (to within the numerical resolution) we still regard the poles above the central object to be a very promising site for the emergence of a GRB fireball.

The amounts of material that become unbound during the coalescence of a slightly asymmetric neutron star system are comparable to those found in previous calculations for symmetric systems ( $\sim 10^{-2}M_{\odot}$  for our most realistic configuration with 1.3 and 1.4  $M_{\odot}$ , no spins and the LS-EOS). However, several uncertainties concerning the amount of ejected material per event enter.

1. *Artificial viscosity (AV)*: The standard form of the artificial viscosity tensor (e.g. Monaghan 1992) is known to create spurious entropy in shear flows. This is of no concern for strictly corotating systems (zero fluid velocity in a corotating frame) but for other spin configurations a shear layer forms at contact. Thus one might suspect that some particles are artificially ejected through spurious forces. However, the AV scheme used in the presented calculations largely suppresses spurious shear forces (in a differentially rotating star the viscous time scales are increased by two orders of magnitude, see appendix) while still keeping the ability to resolve shocks properly. In test calculations without AV for the most probable configuration (non-spinning ns of masses 1.3 and

- 1.4  $M_{\odot}$ ) it turned out that the amount of ejected material ( $10^{-2}M_{\odot}$ ) is definitely *no artifact of the AV scheme*.
2. *Gravity*: The perhaps major shortcoming of the current investigation is the use of Newtonian gravity. It is expected that the deeper general relativistic potentials render the escape of low density material more difficult. Recent Post-Newtonian SPH-calculations (Ayal et al. 1999, Faber & Rasio 1999) support this view. These efforts towards strong-field gravity are undoubtedly steps in the right direction, but it is not immediately obvious how much closer to reality these approaches are since the PN-expansion parameters are  $\sim MR^{-1} \approx 0.2$  at the neutron star surface and thus questionable (Ayal et al. used stars of  $\sim 0.5M_{\odot}$ , Faber and Rasio introduced ad hoc terms to increase the stability of their schemes).  
A further approximation is the use of a point mass back-reaction accounting for forces arising from the emission of gravitational waves. It has to be switched off shortly before the merger. The emission of gravitational waves, however, will still be significant for a short time after the stars first touch (both Ayal et al. and Faber and Rasio find secondary peaks in the gravity wave luminosities) and thus slightly more angular momentum may be radiated away. This might influence the amount of ejecta as well.
  3. *EOS*: The amount of material ejected is extremely sensitive to the nuclear equation of state of the neutron stars. In Rosswog et al. (1999) we found a strong dependence on the stiffness of the EOS (e.g.  $1.5 \cdot 10^{-2}M_{\odot}$  for  $\Gamma = 2.6$  compared to no resolvable mass loss for  $\Gamma = 2.0$ ). Thus we performed test runs with a pseudo-polytropic EOS whose stiffness varied with density. They revealed that the amount of ejecta is basically determined by the behaviour of the nuclear EOS in the high-density regime. This is problematic in two respects. First, the considerable uncertainties in the behaviour of nuclear matter at supranuclear densities constrain our knowledge concerning the ejected material and second, it indicates that the strong-field region in the centre influences the ejecta which are found far away. This might lead one to question the applicability of Newtonian gravity here.

While the first two points (AV, gravity) argue for lower values of the ejected material the last one could decrease (for a softer EOS) as well as increase (stiffer EOS) the amount of ejecta.

Arzoumanian et al. (1999) argue that pulsar ages derived from spin down time scales are generally overestimates and thus birth and merger rates of ns-ns systems are underestimated. They place a firm upper limit of  $10^{-4}\text{yr}^{-1}\text{galaxy}^{-1}$  on the ns-ns merger rate, which agrees with the value estimated by Tutukov and Yungelson (1993) (for a careful discussion of merger rates and their uncertainties see (Fryer et al., 1999)). With this upper limit even an amount as small as  $10^{-4}M_{\odot}$  per event might contribute substantially to the enrichment of the universe with heavy element material (see Fig. 26 in Rosswog et al. 1999).

Concerning the abundance distributions in the ejecta it has to be stressed that fully dynamical r-process calculations using a

realistic EOS, a careful account of weak interactions (including neutrino transport) and a consistent coupling with the hydrodynamic evolution are still lacking. We have performed dynamical r-process network calculations, including heating processes due to the decay of unstable heavy nuclei, that follow the expansion rates of our hydrodynamic calculations (Freiburghaus et al. 1999b; preliminary results are given in Rosswog et al. (1998)). All of the ejected material is found to undergo the r-process. If the initial  $Y_e$  is too low ( $\sim 0.05$ ) the resulting abundance pattern looks s-process like, for  $Y_e = 0.08-0.15$  the solar r-process pattern above the  $A=130$  peak is excellently reproduced, while below this peak non-solar (under-abundant) patterns are found. Thus if the initial  $Y_e$  of the ejecta is in the right range we predict underabundant r-process patterns for nuclei with  $A < 130$  in very old, metal-poor stars, while the nuclei above  $A = 130$  should be found with abundances close to the solar pattern. Actually, there seems to be support for this view coming from observation (Wasserburg et al., 1996; Cowan et al., 1999; Sneden et al., 2000). Since the neutron star merger rate is significantly lower than the core collapse supernova rate, the merger would have to eject more material per event to explain the observations. This would lead to some kind of “clumpyness” in the early distribution of r-process material. Such a clumpyness is actually observed (Sneden et al., 1996): the relative abundances in very old stellar populations match the solar pattern very well, but their absolute values show large variations in different locations.

The main problem for type II supernova ejecta with its high  $Y_e$  values to reproduce the solar r-process pattern stems from the too high entropies that are needed. However, this obstacle might be overcome in the collapsar model. Perhaps here the required entropies could be attained and, depending on the rate and the ejecta per event, an interesting amount of r-process material could be synthesized. However, this r-process scenario might run into problems with the observations of old, metal poor stars due to the short life times of its progenitors and/or the large observed r/Fe ratios reaching values of three times solar. These observations seem to indicate that the emergence of r-process material is delayed with respect to iron (McWilliam et al., 1995; McWilliam, 1997). This delay would disfavour the collapsar model since it is only consistent with low mass SN-progenitors (Mathews et al., 1992), but could find a natural explanation due to the delay caused by the inspiral of a ns-ns binary.

*Acknowledgements.* This work was supported by the Swiss National Science Foundation under grants No. 20-47252.96 and 2000-53798.98 and in part by the National Science Foundation under Grant No. PHY 94-07194 (S.R., F.-K.T.), M.B.D. acknowledges the support of the Royal Society through a University Research Fellowship, T.P. was supported by the US-Israel BSF grant 95-328.

## Appendix A: artificial viscosity

Like other schemes in numerical hydrodynamics SPH uses an artificial viscosity (AV) to resolve shocks properly. The basic task of AV is to keep particles from interpenetrating each other and to ensure the correct solution of the energy equation

across the shock front. If the kinetic energy of matter passing through the shock is not correctly transformed into heat, unphysical oscillations are encountered in the post-shock region. The “standard” SPH viscosity (Monaghan, 1992) allows for an accurate resolution of shock fronts (smoothed over  $\sim 3$  smoothing lengths) and damps out post-shock oscillations. However, since the corresponding AV-tensor (see below) contains terms  $\mathbf{r}_{ij} \cdot \mathbf{v}_{ij}$ , i.e. the inner product of the position and velocity difference vectors of particles  $i$  and  $j$ , spurious forces may be introduced in the case of pure shear flows. SPH has often been criticized for unphysical effects introduced in this way.

Our goal here is to find an AV prescription that is able to resolve shocks properly where necessary, but reduces viscous forces as far as possible in shear flow situations. For a better control of artificial viscosity we suggest here a hybrid scheme that benefits from two recent improvements of the AV treatment in SPH: the introduction of time dependent viscosity parameters  $\alpha$  and  $\beta$  (Morris & Monaghan, 1997) and the so-called Balsara-switch (Balsara, 1995) to suppress viscous forces in pure shear flows. The modified artificial viscosity tensor reads:

$$\Pi_{ij} = \begin{cases} \frac{-\alpha_{ij}(t) c_{ij} \mu_{ij} + \beta_{ij}(t) \mu_{ij}^2}{\rho_{ij}} & \mathbf{r}_{ij} \cdot \mathbf{v}_{ij} \leq 0 \\ 0 & \mathbf{r}_{ij} \cdot \mathbf{v}_{ij} > 0, \end{cases}$$

where  $\beta_{ij} = 2 \cdot \alpha_{ij}$ ,  $\alpha_{ij} = \frac{\alpha_i + \alpha_j}{2}$ ,  $c_{ij} = \frac{c_i + c_j}{2}$ ,  $h_{ij} = \frac{h_i + h_j}{2}$ . The  $c_k$  denote the particle sound velocities,  $h_k$  the smoothing lengths, and  $\mathbf{r}_k$  and  $\mathbf{v}_k$  positions and velocities,  $\mathbf{r}_{ij} = \mathbf{r}_i - \mathbf{r}_j$ ,  $\mathbf{v}_{ij} = \mathbf{v}_i - \mathbf{v}_j$ . The term that is responsible for possibly spurious effects is modified by the Balsara-switch:

$$\mu_{ij} = \frac{h_{ij} \mathbf{r}_{ij} \cdot \mathbf{v}_{ij}}{r_{ij}^2 + \eta h_{ij}^2} \cdot \frac{f_i + f_j}{2}, \quad (\text{A.1})$$

where  $\eta = 0.01$  and

$$f_i = \frac{|\nabla \cdot \mathbf{v}|_i}{|\nabla \cdot \mathbf{v}|_i + |\nabla \times \mathbf{v}|_i + \eta' c_i / h_i}. \quad (\text{A.2})$$

The SPH-prescription for the velocity curl is:

$$(\nabla \times \mathbf{v})_i = \frac{1}{\rho_i} \sum_j m_j \mathbf{v}_{ij} \times \nabla_i W_{ij} \quad (\text{A.3})$$

and the velocity divergence is given by

$$(\nabla \cdot \mathbf{v})_i = -\frac{1}{\rho_i} \sum_j m_j \mathbf{v}_{ij} \cdot \nabla_i W_{ij} \quad (\text{A.4})$$

In a pure shock the divergence term will dominate over the curl,  $|\nabla \cdot \mathbf{v}|_i \gg |\nabla \times \mathbf{v}|_i$ , and thus  $f_i \rightarrow 1$ , reproducing the standard viscosity term. In pure shear flows, however, the curl dominates,  $|\nabla \times \mathbf{v}|_i \gg |\nabla \cdot \mathbf{v}|_i$ , and thus strongly suppresses viscous terms since  $f_i \rightarrow 0$ . To prevent numerical divergences  $\eta' (= 10^{-4})$  is introduced.

To have enough viscosity where it is needed, i.e. to resolve shocks properly, but to keep it on a minimal level otherwise the viscosity parameters  $\alpha$  and  $\beta (= 2\alpha)$  are allowed to evolve in time. This is realized by determining the viscosity coefficient  $\alpha_i$  from an additional equation that has to be integrated together

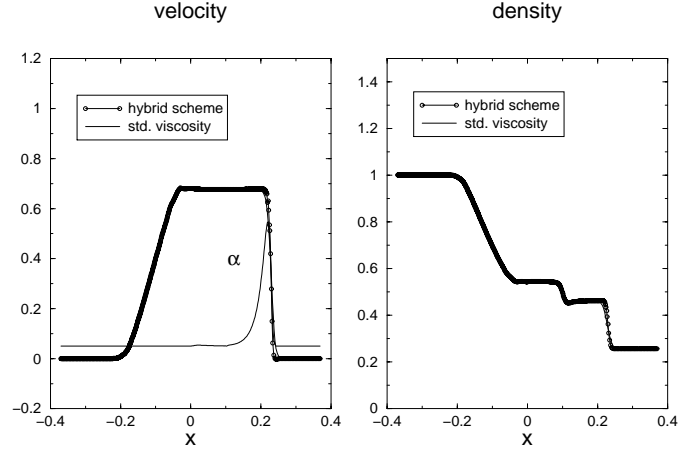


**Fig. A.1.** Comparison of shock tube results at  $t = 0.15$  between the standard SPH artificial viscosity ( $\alpha = 1, \beta = 2$ ) and our hybrid AV scheme ( $\alpha_{max} = 1.5, \alpha_{min} = 0.05, c = 0.2$ ). The time dependent viscosity parameter  $\alpha$  is also shown in the left panel.

with the other dynamic equations. It contains a term that drives the decay towards minimum values  $\alpha_{min}$  on a time scale  $\tau_i$  and a source term  $S_i$  responsible for the rise of the parameters in the presence of shocks:

$$\frac{d\alpha_i}{dt} = -\frac{\alpha_i - \alpha_{min}}{\tau_i} + S_i. \quad (\text{A.5})$$

To keep the viscosity parameters in a well-defined interval and to allow for sufficiently *fast* rise if a shock is detected, we have slightly modified the original source term equation:

$$S_i = \max(-(\nabla \cdot \mathbf{v})_i (\alpha_{max} - \alpha_i), 0), \quad (\text{A.6})$$

After a number of numerical experiments we have chosen the following parameters whose appropriateness will be shown in the subsequent tests:  $\alpha_{max} = 1.5$ ,  $\alpha_{min} = 0.05$  and  $\tau_i = \frac{h_i}{\epsilon c_i}$  with  $\epsilon = 0.2$ .

To validate this form of AV we compare its capabilities to the standard scheme in the context of three test cases: (i) a 1D shock tube to test the ability to resolve shocks, (ii) a stationary, differentially rotating star where viscous time scales are calculated to quantify the amount of spurious shear forces and (iii) a close, tidally interacting non-equilibrium binary neutron star system that is driven to the dynamical instability limit by viscosity.

For the shock tube test we start with the initial conditions described in (Hernquist & Katz, 1989) (see also references therein):

$$\begin{aligned} \rho &= 1, & P &= 1, & v &= 0 & \text{for } x < 0 \\ \rho &= 0.25, & P &= 0.1795, & v &= 0 & \text{for } x \geq 0 \end{aligned} \quad (\text{A.7})$$

with a ratio of specific heats  $\gamma = 1.4$  and 1000 equal mass particles with  $m_i = 0.75/1000$  initially distributed in a way that (A.7) is satisfied. Smoothing lengths are fixed to  $h_i = 0.0065$ . In Fig. A.1 we show a comparison of the density and velocity profiles at  $t = 0.15$  between the standard AV with  $\alpha = 1$  and

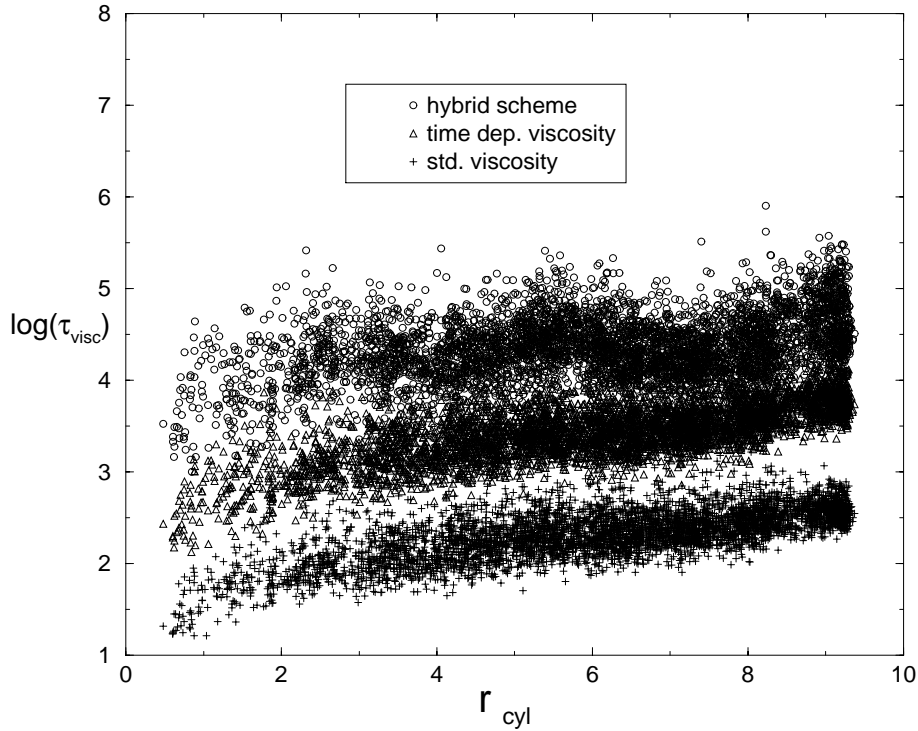


**Fig. A.2.** Viscous time scales  $\tau_{visc,i} = v_i/\dot{v}_{i,visc} = v_i/(|\sum_j m_j \Pi_{ij} \nabla_i W_{ij}|)$  in a differentially rotating equilibrium configuration for the standard AV, the time dependent scheme of Morris and Monaghan ( $\alpha_{max} = 1.5, \alpha_{min} = 0.05, c = 0.2$ ) and the hybrid scheme used here. All quantities are given in code units ( $G = c = M_\odot = 1$ ).

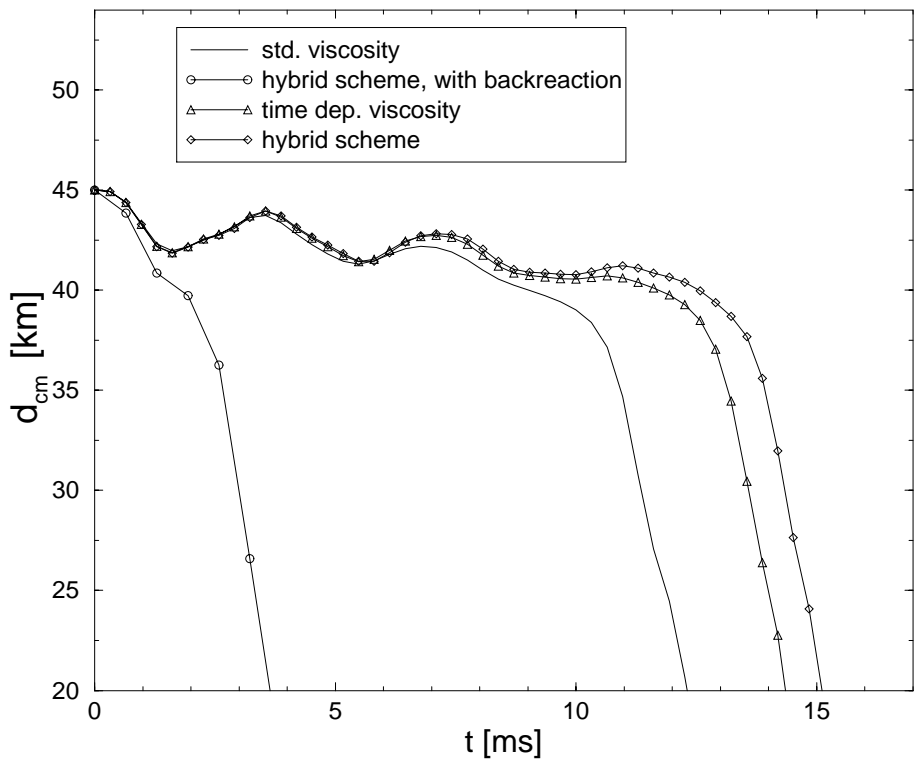


**Fig. A.3.** Evolution of the distance between the centers of mass of an irrotational system (both stars with  $1.4 M_\odot$ ). Apart from one test case (circles) the inspiral is entirely driven by viscosity.

$\beta = 2$  (often suggested as “standard” values, see e.g. Monaghan 1992) and our hybrid scheme. The hybrid scheme shows a slightly sharper resolution of the shock front, apart from that the calculated shock-profiles are almost indistinguishable. The time dependent viscosity parameter  $\alpha$  is also displayed in the left panel. It is sharply peaked at the shock front where it reaches

values of  $\approx 0.6$  and is close to the minimum value of 0.05 otherwise. In summary, the hybrid scheme exhibits shock resolution capabilities very similar to the standard scheme, but the average value of the viscosity parameter  $\alpha$  is largely reduced.

In a second, 3D, test we will focus on shear flows in a configuration specific to our merger application. To this end

we construct a stationary, differentially rotating star in a way similar to Lombardi et al. (Lombardi et al., 1999): (i) we start from a relaxed spherical star obeying the LS-EOS, (ii) give all the particles a constant velocity  $v_0 = 0.1c$ , i.e. the star rotates differentially with  $\omega(r) \sim r_{cyl}^{-1}$ , where  $r_{cyl}$  is the distance to the rotation axis, (iii) to reach a rotating equilibrium state, unwanted velocities are damped out by applying an artificial drag force  $\mathbf{f}_d \sim (v_0 \cdot \hat{e}_\phi - \mathbf{v}_i)$ . A star relaxed in this way exhibits a  $\omega$ -profile close to  $\sim r_{cyl}^{-1}$ , only near the origin, where the kernels overlap, the  $\omega$ -singularity is smoothed to finite values. In a totally inviscid star, the viscous times scales  $\tau_{visc,i} = v_i / \dot{v}_{i,visc} = v_i / (|\sum_j m_j \Pi_{ij} \nabla_i W_{ij}|)$  should be infinite. However, by means of the terms in the artificial viscosity tensor that contain  $\mathbf{v}_{ij} \cdot \mathbf{r}_{ij}$  spurious viscous forces are introduced in pure shear flows that lead to finite viscous time scales. Thus, the aim of an improved viscosity scheme has to be the increase of these  $\tau_{visc,i}$ . For a differentially rotating equilibrium configuration with 5000 particles constructed in the three steps described above the viscous time scale  $\tau_i$  of each particle is shown in Fig. A.2 as a function of the distance to the rotation axis  $r_{cyl}$ . Plus signs refer to the standard viscosity ( $\alpha = 1, \beta = 2$ ), triangles to a time dependent scheme ( $\alpha_{max} = 1.5, \alpha_{min} = 0.05, c = 0.2$ ), and circles to the hybrid scheme (time dependent  $\alpha$  and Balsara switch). The introduction of time dependent viscosity parameters alone increases the viscous times (for the chosen parameter set) by approximately one order of magnitude. The additional Balsara switch further improves the time scales by another order of magnitude.

In our last, 3D test we start out from a close binary system where both stars have  $1.4 M_\odot$ , an initial separation  $a_0 = 45$  km and do not possess any spin. Since the initial stars are spherical and the system is close enough for tidal interaction the binary components start to oscillate and thereby transform orbital energy into oscillatory energy. Since we are interested here in (spurious) effects of viscosity, the initial system is not provided with radial velocities, no gravitational backreaction force is applied during this calculation. The inspiral and final merger is triggered by viscosity alone. In Fig. A.3 the evolution of the center of mass distance of the binary is shown (10000 particles). For reasons of comparison the evolution of a system with initial radial velocities and backreaction force is also displayed. The introduction of time dependent AV parameters substantially delays the time until the system becomes dynamically unstable, the additional Balsara-factor further retards the coalescence.

## References

- Abramovici A., et al., 1992, *Science* 256, 325  
 Akmal A., Pandharipande V., Ravenhall D., 1998, *Phys. Rev. C* 58, 1804  
 Aloy M., Müller E., Ibanez J., Marti J., MacFadyen A., 1999, *ApJ*, L119  
 Arzoumanian Z., Cordes J.M., Wasserman I., 1999, *ApJ* 520, 696  
 Ayal S., Piran T., Oechslin R., Davies M.B., Rosswog S., 1999, in 23 pages, 12 figures, uses aastex v5, submitted to *ApJ*, pp 10154+  
 Balsara D., 1995, *J. Comput. Phys.* 121, 357  
 Baumgarte T., Cook G., Scheel M., Shapiro S., Teukolsky S., 1997, *Phys. Rev. Lett.* 79, 1182  
 Baumgarte T., Cook G., Scheel M., Shapiro S., Teukolsky S., 1998a, *Phys. Rev. D* 57, 6181  
 Baumgarte T., Cook G., Scheel M., Shapiro S., Teukolsky S., 1998b, *Phys. Rev. D* 57, 7299  
 Benz W., 1990, in: Buchler J. (ed.), *Numerical Modeling of Stellar Pulsations*, p. 269, Dordrecht: Kluwer Academic Publishers  
 Benz W., Bowers R., Cameron A., Press W., 1990, *ApJ* 348, 647  
 Bildsten L., Cutler C., 1992, *ApJ* 400, 175  
 Blanchet L., Damour T., Schäfer G., 1990, *MNRAS* 242, 289  
 Blandford R.D., Helfand D.J., 1999, *MNRAS* 305, L45  
 Bodenheimer P., Woosley S.E., 1983, *ApJ* 269, 281  
 Bonazzola S.,ourgoulhon E., Marck J., 1999, *Phys. Rev. Lett.* 82, 892  
 Bradaschia C., et al., 1990, *Nucl. Instrum. Methods Phys. Res. A* 289, 518  
 Costa E., et al., 1997, *Nat* 387, 783  
 Cowan J.J., Sneden C., Ivans I., et al., 1999, in *American Astronomical Society Meeting*, Vol. 194, pp. 6704+  
 Davies M., Benz W., Piran T., Thielemann F.-K., 1994, *ApJ* 431, 742  
 Djorgovski S., et al., 1997, *Nat* 387, 876  
 Eichler D., Livio M., Piran T., Schramm D.N., 1989, *Nat* 340, 126  
 Faber J.A., Rasio F.A., 1999, in *RevTeX*, 37 pages, 17 figures, submitted to *Phys. Rev. D*, pp 12097+  
 Frail D., et al., 1997, *Nat* 389, 261  
 Freiburghaus C., Kolbe E., Rauscher T., et al., 1997, in: Görres J., Mathews g., Shore S., Wiescher M. (eds.), *Proc. 4th Int. Symp. on Nuclei in the Cosmos (Univ. of Notre Dame)*, Vol. A621, p. 405c, *Nuc. Phys.*  
 Freiburghaus C., Rembges J., Rauscher T., et al., 1999a, *ApJ* 516, 381  
 Freiburghaus C., Rosswog S., Thielemann F.-K., 1999b, *ApJ* 525, L121  
 Fryer C., Burrows A., Benz W., 1998, *ApJ* 496, 333  
 Fryer C., Kalogera V., 1997, *ApJ* 489, 244  
 Fryer C.L., Woosley S.E., Hartmann D.H., 1999, *ApJ* 526, 152  
 Galama T., et al., 1997, *Nat* 387, 479  
 Galama T.J., Vreeswijk P.M., van Paradijs J., et al., 1998, *Nat* 395, 670  
 Hernquist L., Katz N., 1989, *ApJS* 70, 419  
 Hoffman R.D., Woosley S.E., Qian Y.-Z., 1997, *ApJ* 482, 951  
 Iwamoto K., Mazzali P.A., Nomoto K., et al., 1998, *Nat* 395, 672  
 Janka H.T., Ruffert M., 1998, in: *Proceedings of the 9th workshop on Nuclear Astrophysics*, pp 94+  
 Kalogera V., Baym G., 1996, *ApJ* 470, L61  
 Kluzniak W., Lee W.H., 1998, *ApJ* 494, L53  
 Kochanek C., 1992, *ApJ* 398, 234  
 Kuroda K., et al., 1997, in: *Gravitational Wave Detection, Proceedings of the TAMA International Workshop on Gravitational Wave Detection*, *Frontiers Science Series No. 20*. Universal Academy Press, Inc., 1997., p.309, pp 309  
 Lai D., 1994, *MNRAS* 270, 611  
 Lai D., 1996, *Phys. Rev. Lett.* 76, 4878  
 Lai D., Rasio F., Shapiro S., 1993a, *ApJS* 88, 205  
 Lai D., Rasio F., Shapiro S., 1993b, *ApJ* 406, L63  
 Lai D., Rasio F., Shapiro S., 1994a, *ApJ* 420, 811  
 Lai D., Rasio F., Shapiro S., 1994b, *ApJ* 423, 344  
 Lai D., Rasio F., Shapiro S., 1994c, *ApJ* 437, 742  
 Lai D., Wiseman A., 1997, *Phys. Rev. D* 54, 3958  
 Lattimer J.M., Schramm D.N., 1974, *ApJ* 192, L145  
 Lattimer J.M., Schramm D.N., 1976, *ApJ* 210, 549  
 Lattimer J.M., Swesty F.D., 1991, *Nucl. Phys. A* 535, 331  
 Lattimer J.M., Yahil A., 1989, *ApJ* 340, 426

- Lombardi J., Rasio F., Shapiro S., 1997, *Phys. Rev. D* 56, 3416
- Lombardi J., Sills A., Rasio F., Shapiro S., 1999, *J. Comp. Phys.* 152, 687
- Luck H., 1997, *Class. Quant. Grav.* 14, 1471
- MacFadyen A.I., Woosley S.E., 1999, *ApJ* 524, 262
- Mathews G., Wilson J.R., 1997, *ApJ* 482, 929
- Mathews G.J., Bazan G., Cowan J., 1992, *ApJ* 391, 719
- McLaughlin G., Fetter J., Balantekin A., Fuller G., 1999, *Phys. Rev. C* 59, 2873
- McWilliam A., 1997, *ARA&A* 35, 503
- McWilliam A., Preston G.W., Sneden C., Searle L., 1995, *AJ* 109, 2757+
- Meyer B.S., 1989, *ApJ* 343, 254
- Meyer B.S., Brown J.S., 1997, *ApJ* S112, 199
- Meyer B.S., McLaughlin G., Fuller G., 1998, *Phys. Rev. C* 58, 3696
- Monaghan J., 1992, *Ann. Rev. Astron. Astrophys.* 30, 543
- Morris J., Monaghan J., 1997, *J. Comp. Phys.* 136, 41
- New K.C.B., Tohline J.E., 1997, *ApJ* 490, 311
- Paczyński, B., 1998, *ApJ* 494, L45
- Paradijs J.V., et al., 1997, *Nat* 386, 686
- Peters P., Mathews J., 1963, *Phys. Review* 131, 435
- Peters P., Mathews J., 1964, *Phys. Review* B136, 1224
- Rasio F., Shapiro S., 1992, *ApJ* 401, 226
- Rasio F., Shapiro S., 1994, *ApJ* 432, 242
- Rasio F., Shapiro S., 1995, *ApJ* 438, 887
- Rasio F., Shapiro S., 1999, *CQG* 16, R1
- Rosswog S., Freiburghaus C., Thielemann F.-K., 1998, in: *Proc. Nuclei in the Cosmos V*, Volos, Greece, July 1998
- Rosswog S., Liebendörfer M., Thielemann F.-K., et al., 1999, *A&A* 341, 499
- Ruffert M., Janka H., Schäfer G., 1996, *A&A* 311, 532
- Ruffert M., Janka H., Takahashi K., Schäfer G., 1997, *A&A* 319, 122
- Ruffert M., Janka H.T., 1999, *A&A* 344, 573
- Sahu K., et al., 1997, *Nat* 387, 476
- Shapiro S., Teukolsky S.A., 1983, *Black Holes, White Dwarfs and Neutron Stars*, New York: Wiley & Sons
- Shemi A., Piran T., 1990, *ApJ* 379, L17
- Shen H., Toki H., Oyamatsu K., Sumiyoshi K., 1998, *Nuclear Physics A* 637, 435
- Shibata M., 1996, *Prog. Theor. Phys.* 96, 317
- Shibata M., Baumgarte T., Shapiro S., 1998, *Phys. Rev. D* 58, 23002
- Shibata M., Nakamura T., Oohara K., 1993, *Prog. Theor. Phys.* 89, 809
- Shibata M., Taniguchi K., 1997, *Phys. Rev. D* 56, 811
- Sneden C., McWilliam A., Preston G.W., et al., 1996, *ApJ* 467, 819
- Sneden C., et al., 2000, *ApJ* 533, L1395
- Stark R., Piran T., 1985, *Phys. Rev. Lett.* 55, 891
- Symbalisty E.M.D., Schramm D.N., 1982, *Astrophys. Lett.* 22, 143
- Takahashi K., Witt J., Janka H.-T., 1994, *A&A* 286, 857
- Taniguchi K., Nakamura T., 1996, *Prog. Theor. Phys.* 96, 693
- Taniguchi K., Shibata M., 1997, *Phys. Rev. D* 56, 798
- Thorsett S., 1996, *Phys. Rev. Lett.* 77, 1432
- Thorsett S., Chakrabarti 1999, *ApJ* 7512, 288
- Tutukov A., Yungelson L., 1993, *Astronomicheskii Zhurnal* 70, 812
- Wasserburg G., Busso M., Gallino R., 1996, *ApJ* 466, L109
- Weber F., Glendenning N., 1992, *ApJ* 390, 541
- Wheeler J.C., Hoeflich P., Wang L., 1998, in: *American Astronomical Society Meeting*, Vol. 193, pp 4206+
- Wilson J.R., Mathews G., 1995, *Phys. Rev. Lett.* 75, 4161
- Wilson J.R., Mathews G., Marronetti P., 1996, *Phys. Rev. D* 54, 1317
- Woosley S.E., 1993, *ApJ* 405, 273
- Zhuge X., Centrella J., McMillan S., 1994, *Phys. Rev. D* 50, 6247
- Zhuge X., Centrella J., McMillan S., 1996, *Phys. Rev. D* 54, 7261